crystals

MDPI

Article

Evidence of Counterion Size Effect on the Stability of Columnar Phase of Ionic Liquid Crystals Based on Pyridinium Salts Derived from *N*-3,4,5-Tri(alkyloxy)-benzyl-4-pyridones

Isabela Dumitru [1], Florentina L. Chiriac [1], Monica Ilis [1], Iuliana Pasuk [2], Doina Manaila-Maximean [3], Marin Micutz [4], Teodora Staicu [4] and Viorel Cîrcu [1,*]

[1] Department of Inorganic Chemistry, University of Bucharest, 4-12 Regina Elisabeta Blvd., 030018 Bucharest, Romania; oceansoul76@yahoo.com (I.D.); laura.badea88@yahoo.com (F.L.C.); monica.ilis@chimie.unibuc.ro (M.I.)
[2] National Institute of Materials Physics, P.O. Box MG-7, 077125 Magurele, Romania; iuliana.pasuk@ifim.ro
[3] Department of Physics, University Politehnica of Bucharest, Spl. Independentei 313, 060042 Bucharest, Romania; doina.manaila@upb.ro
[4] Department of Physical Chemistry, University of Bucharest, 4-12 Regina Elisabeta Blvd., 030018 Bucharest, Romania; marin.micut@chimie.unibuc.ro (M.M.); teos@gw-chimie.math.unibuc.ro (T.S.)
* Correspondence: viorel.circu@chimie.unibuc.ro

Abstract: The synthesis and characterization of novel ionic liquid crystals based on pyridinium salts with Br^- and PF_6^- counterions are described in this work. These pyridinium salts were derived from 4-hydroxypyridine, both by *N*- and *O*-alkylation. The 3,4,5-tri(alkyloxy)-benzyl mesogenic unit was attached to the nitrogen atom of the pyridinium ring. Alkyl chains with a different number of carbon atoms (6, 8, 10, 12 and 14) were employed in order to show the effect on the stability of mesophase. The POM (polarizing optical microscopy) and XRD (powder X-ray diffraction) studies indicated that bromide salts with shorter chains C_6, C_8 and C_{10} do not show mesomorphic properties, while longer chain analogues with C_{12} and C_{14} exhibit two enantiotropic columnar phases. Surprisingly, the pyridinium salts with the larger size PF_6^- counterion do not exhibit liquid crystal properties.

Keywords: liquid crystals; ionic liquid crystals; pyridinium salts; 4-pyridone; columnar phase

check for updates

Citation: Dumitru, I.; Chiriac, F.L.; Ilis, M.; Pasuk, I.; Manaila-Maximean, D.; Micutz, M.; Staicu, T.; Cîrcu, V. Evidence of Counterion Size Effect on the Stability of Columnar Phase of Ionic Liquid Crystals Based on Pyridinium Salts Derived from *N*-3,4,5-Tri(alkyloxy)-benzyl-4-pyridones. *Crystals* **2022**, *12*, 715. https://doi.org/10.3390/cryst12050715

Academic Editors: Charles Rosenblatt, Ingo Dierking and Benoit Heinrich

Received: 8 April 2022
Accepted: 13 May 2022
Published: 17 May 2022

Publisher's Note: MDPI stays neutral with regard to jurisdictional claims in published maps and institutional affiliations.

Copyright: © 2022 by the authors. Licensee MDPI, Basel, Switzerland. This article is an open access article distributed under the terms and conditions of the Creative Commons Attribution (CC BY) license (https://creativecommons.org/licenses/by/4.0/).

1. Introduction

Ionic liquid crystals (ILCs) are a distinct class of liquid crystals that have been known about for a long time. They generally consist of a positively charged cationic core and at least one long alkyl chain. These versatile materials combine the liquid crystals with ionic liquids properties. More importantly, they combine anisotropy of physical properties with ionic conductivity and low volatility [1,2]. Thus, for ILC materials, the formation of liquid crystalline (LC) phases is determined by the microphase segregation of polar (cationic core) and nonpolar (alkyl groups) domains. Several factors are known to lead to the partially ordered environments of the LC phase. These are the hydrogen bonding between cations and anions [3–5] and the van der Waals, electrostatic, hydrophobic and dipole-dipole interactions [6,7]. To obtain the ionic liquid crystals, the design of a conventional liquid crystal could be developed by the introduction of the desired ionic groups together with traditional mesogenic groups (mostly long alkyl chains, cyanobiphenyl units, etc.). The imidazolium, pyridinium and phosphonium cores are the most attractive candidates for this task, particularly due to their relatively easy synthetic pathways [8,9]. On the other hand, although most of the studies reported in the literature were focused on the halide salts (with bromide, chloride, or iodide anions), other counterions were also used to prepare ILCs. In many examples, these counterions have a larger size and their appropriate choice is intended to control the liquid crystalline properties or to tailor the specific applications, including the decrease in the melting points and the viscosity of the products. In this respect, many reports are dedicated to the prediction of the properties of new ILCs made

through joining together known constituents, and these studies offer important knowledge on the rational design of these materials. The size of counterions was found to play a vital role in the stabilization and the type of the mesophases exhibited by ILCs [10–12]. Besides the halide anions, commonly used anions to obtain single charged ILCs are perfluorinated anionic species such as BF_4^-, PF_6^- and $CF_3SO_3^-$.

The pyridinium-based ILCs are intensively investigated as these products exhibit very similar properties to the related popular imidazolium-based ILCs [13–22]. The use of pyridinium core generates a variety of molecular shapes, from calamitic to discotic materials and various liquid crystalline phases ranging from the less common nematic phase to the most commonly observed SmA phase for ionic mesogens or hexagonal columnar phases. The mesomorphic behavior of the pyridinium-based ILCs is dictated by the position and the nature of the mesogenic groups attached to the pyridinium ring, as well as the counterion employed [23,24]. Several recent reviews focused on this topic [25,26].

In this paper, we report the synthesis and the characterization of a new series of pyridinium salts obtained from 4-hydroxypyridine as a starting material and containing on one side a 3,4,5-tri(alkyloxy)benzyl mesogenic unit and on the other side an alkyloxy group, using different counterions. The 4-hydroxypiridine precursor is well known for its ability to give both *O*- and *N*-alkylated pyridinium salts [27]. In the first step 4-hydroxypyridine has been mono *N*-alkylated to obtain the neutral *N*-(3,4,5-trialkyloxybenzyl)-4-pyridones compounds, followed by a further *O*-alkylation of these compounds with different alkyl halides to yield the *N*-(3,4,5-trialkyloxybenzyl)-4-alkoxypyridinium bromide salts as new ILCs. Further, the exchange of the bromide anion with PF_6^- counterion provided the new family of related pyridinium salts. Our preliminary results on the C_{12} analogues revealed that replacing bromide ion (Br^-) with other counterions (NO_3^-, BF_4^- and PF_6^-) resulted in mesophase suppression [28]. The destabilization effect of the liquid crystal phase due to the use of larger counterions, such as tetrafluoroborate and hexafluorophosphate, could be, in principle, compensated by employing longer alkyl chains. For this purpose, in this study, longer C_{14} analogues have been prepared and investigated along with shorter analogues (C_6, C_8 and C_{10}) in combination with PF_6^- fluorinated counterion. The molecular structures, liquid crystalline properties, thermal stability, and optical properties have been investigated by various experimental techniques, providing pertinent and exhaustive insights into the structural factors that were correlated with the stability of the liquid crystalline phases of the new pyridinium-based ILCs.

2. Materials and Methods

2.1. Materials and Measurements

All the chemicals, reagents and common solvents were supplied from Sigma-Aldrich and Merck and used as received without further purification. The synthesis and characterization of the 4-pyridone intermediates were described by us in previous reports [28,29].

^{1}H-NMR (300 MHz) and ^{13}C-RMN (75 MHz) spectra were obtained with a Bruker Fourier 300 or Bruker Avance III spectrometer (Bruker BioSpin NMR, Rheinstetten, Germany) using $CDCl_3$ as a solvent. C, H, N analyses were carried out with an EuroEA 3300 (Eurovector, Pavia, Italy) instrument after drying of the samples in a vacuum. IR spectra of the samples in solid state were measured by the ATR method performed on a Bruker Tensor V-37 spectrophotometer (Bruker Optics Inc., Billerica, MA, USA) in the range of 4000–400 cm^{-1}. The liquid crystal properties were characterized by differential scanning calorimetry using a Diamond DSC Perkin Elmer instrument (Perkin Elmer, Boston, MA, USA) operating at a scanning rate of 10 °C/min. Samples were encapsulated in aluminum pans and kept in a dry nitrogen atmosphere. Polarizing optical microscopy (POM) observations of transitions and optical textures on untreated glass slides were carried out with a Nikon 50iPol polarized optical microscope (Nikon Instruments, Melville, NY, USA) equipped with a Linkam THMS600 hot stage and TMS94 control processor (Linkam Scientific Instruments Ltd., Tadworth, UK). XRD measurements of the samples were characterized on cooling from the isotropic state by a D8 Advance diffractometer

(Bruker AXS GmbH, Karlsruhe, Germany) in parallel beam setting with monochromatized Cu–$K_{\alpha 1}$ radiation (λ = 1.5406 Å), a scintillation detector, and a horizontal sample stage. A home-made heating stage adapted to the sample stage of the diffractometer was used for temperature control of the sample during the measurements. The samples were heated and cooled with a rate of 10.0 °C/min to the corresponding temperature.

2.2. Synthesis of Bromide Pyridinium Salts, **2a–e**

The quaternary bromide pyridinium salts were obtained by the alkylation reaction between 4-pyridone derivatives, **1a–e,** (1 g, 2.06 mmol) in acetonitrile and the corresponding bromoalkane (excess of $C_nH_{2n+1}Br$, n = 6, 8, 10, 12, 14; 6.8 mmol) under reflux in nitrogen atmosphere for 48 h (Scheme 1). After this period, the solvent was evaporated to dryness. The obtained product was purified on silica gel column chromatography using as eluent a mixture of DCM/MeOH (95:5), followed by its recrystallization from DCM and ethyl ether, resulting in white solids.

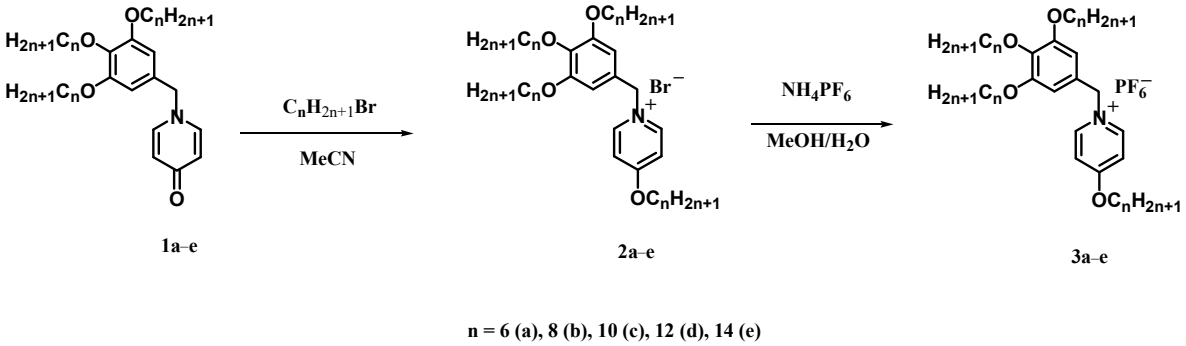

Scheme 1. Preparation of the pyridinium salts discussed in this study.

2a: ^{1}H-NMR ($CDCl_3$, 300 MHz): 9.24 (d, *J* = 7.3 Hz, 2H); 7.24 (m, 2H); 6.86 (s, 2H); 5.89 (s, 2H), 4.19 (t, *J* = 6.4 Hz, 2H); 3.92 (m, 6H); 2.00–1.57 (m, 8H); 1.48–1.27 (m, 24H); 0.87 (m, 12H). ^{13}C-NMR ($CDCl_3$, 75 MHz): 170.20, 153.76, 146.02, 138.89, 128.05, 113.44, 107.84, 73.37, 71.49, 69.42, 62.50, 31.61, 31.24, 30.20, 29.28, 28.30, 25.70, 25.25, 24.18, 22.52, 19.73, 13.88. IR (ATR, cm^{-1}): 2928, 2858, 1642, 1591, 1520, 1467, 1443, 1329, 1255, 1110, 849, 728. Yield: 72%. Anal. Calcd for $C_{36}H_{60}BrNO_4x0.5H_2O$: C% 65.53, H% 9.32, N% 2.12. Anal. Found: C% 65.14, H% 9.69, N% 2.05.

2b: ^{1}H-NMR ($CDCl_3$, 300 MHz): 9.21 (d, *J* = 7.2 Hz, 2H); 7.24 (m, 2H); 6.85 (s, 2H); 5.89 (s, 2H); 4.32–4.14 (m, 2H); 3.95 (m, 6H); 1.90–1.66 (m, 8H); 1.28 (m, 40H); 0.88 (t, *J* = 6.5 Hz, 12H). ^{13}C-NMR ($CDCl_3$, 75 MHz): 170.21, 153.78, 145.99, 138.91, 128.02, 113.43, 107.85, 73.41, 71.50, 69.44, 62.53, 31.77, 30.28, 29.62, 28.91, 28.36, 26.07, 25.60, 22.59, 14.03. IR (ATR, cm^{-1}): 2926, 2855, 1641, 1590, 1521, 1465, 1443, 1329, 1255, 1112, 850, 724. Yield: 75%. Anal. Calcd for $C_{44}H_{76}BrNO_4x0.5H_2O$: C% 68.46, H% 10.05, N% 1.81. Anal. Found: C% 68.09, H% 10.38, N% 1.72.

2c: ^{1}H-NMR ($CDCl_3$, 300 MHz): 9.17 (d, *J* = 7.2 Hz, 2H); 7.24 (m, 2H); 6.79 (s, 2H); 5.85 (s, 2H), 4.21 (t, *J* = 6.5 Hz, 2H); 3.94 (m, 6H); 1,77 (m, 8H); 1.26 (m, 56H); 0.87 (t, *J* = 6.7 Hz, 12H). ^{13}C-NMR ($CDCl_3$, 75 MHz): 171.23, 153.79, 145.87, 113.48, 107.92, 73.39, 71.52, 69.49, 62.58, 31.85, 29.84, 28.90, 28.35, 26.10, 22.65, 14.08. IR (ATR, cm^{-1}): 2920, 2851, 1639, 1592, 1516, 1468, 1446, 1314, 1254, 1129, 849, 721. Yield: 73%. Anal. Calcd for $C_{52}H_{92}BrNO_4x0.5H_2O$: C% 70.63, H% 10.60, N% 1.58. Anal. Found: C% 70.27, H% 10.85, N% 1.49.

2d: ^{1}H-NMR ($CDCl_3$, 300 MHz): 9.18 (d, *J* = 7.2 Hz, 2H); 7.24 (m, 2H); 6.81(s, 2H); 5.85 (s, 2H); 4.19 (t, 2H); 3.93 (m, 6H); 1.87–1.67 (m, 8H); 1.45–1.20 (m, 72H); 0.86 (m, 12H). ^{13}C-NMR ($CDCl_3$, 75 MHz): 170.24, 153.81, 145.97, 138.96, 127.98, 113.46, 107.88, 73.38, 71.51, 69.48, 62.60, 31.91, 30.31, 29.70, 29.62, 29.48, 29.41, 25.64, 22.67, 14.09. IR (ATR, cm^{-1}): 2956,

2918, 2850, 1640, 1593, 1517, 1469, 1446, 1314, 1255, 1129, 846, 720. Yield: 77%. Analytical data reported in [28].

2e: ^{1}H-NMR ($CDCl_3$, 300 MHz): 9.18 (d, *J* = 7.1 Hz, 2H); 7.24 (m, 2H); 6.81 (s, 2H); 5.85 (s, 2H), 4.28–4.04 (m, 2H); 4.04–3.81 (m, 6H); 1.96–1.57 (m, 8H); 1.24 (m, 88H); 0.85 (t, *J* = 6.9 Hz, 12H). ^{13}C-NMR (75 MHz, $CDCl_3$) δ 170.22, 153.81, 146.00, 138.96, 127.98, 113.43, 107.88, 73.38, 71.43, 69.46, 62.61, 31.90, 30.32, 29.87, 28.91, 28.39, 26.11, 25.63, 22.66, 14.09. IR (ATR, cm^{-1}): 2917, 2849, 1640, 1592, 1519, 1469, 1444, 1307, 1255, 1121, 845, 720. Yield: 81%. Anal. Calcd for $C_{68}H_{124}BrNO_4xH_2O$: C% 73.08, H% 11.36, N% 1.25. Anal. Found: C% 72.78, H% 11.85, N% 1.07.

2.3. Synthesis of PF_6^- Pyridinium Salts, **3a–e**

Pyridinium salts **3a–e** were obtained by the metathesis reaction between bromide salts **2a–e** (0.155 mmol), dissolved in methanol (5 mL) and an equivalent amount of NH_4PF_6 (0.026 g, 0.155 mmol) dissolved in 3 mL water. The reaction mixture was stirred at room temperature for 1 h. The resulting precipitate was filtered, washed with methanol and recrystallized from CH_2Cl_2/Et_2O.

3a: ^{1}H-NMR ($CDCl_3$, 300 MHz): 8.48 (d, *J* = 6.9 Hz, 2H); 7.25 (m, 2H); 6.65 (s, 2H); 5.42 (s, 2H); 4.20 (t, *J* = 6.4Hz, 2H); 3.97 (m, 6H), 1.87–1.67 (m, 8H); 1.45–1.20 (m, 24H); 0.88 (m, 12H). ^{13}C-RMN ($CDCl_3$, 75 MHz): 170.58, 154.01, 145.07, 139.16, 127.09, 113.72, 107.48, 73.42, 71.46, 69.32, 63.57, 31.80, 31.68, 30.32, 29.71, 29.30, 28.35, 26.10, 25.60, 22.63, 14.07. IR (ATR, cm^{-1}): 2956, 2932, 2860, 1644, 1592, 1524, 1468, 1444, 1325, 1252, 1111, 859, 728, 557. Yield: 69%. Anal. Calcd for $C_{36}H_{60}F_6NO_4P$: C% 62.46, H% 8.88, N% 2.02. Anal. Found: C% 62.72, H% 9.10, N% 1.97.

3b: ^{1}H-NMR ($CDCl_3$, 300 MHz): 8.49 (d, *J* = 7.1 Hz, 2H); 7.22 (d, *J* = 7.1 Hz, 2H); 6.61 (s, 2H); 5.38 (s, 2H), 4.20 (t, *J* = 6.5 Hz, 2H); 3.93 (m, 6H), 1.77 (m, 8H); 1.33 (m, 40H); 0.87 (m, 12H).^{13}C-NMR ($CDCl_3$, 75 MHz): 170.59, 154.02, 145.09, 139.15, 127.09, 113.70, 107.50, 73.42, 71.49, 69.29, 63.57, 31.80, 31.70, 30.32, 29.53, 29.39, 29.20, 29.10, 28.93, 28.37, 26.07, 25.60, 22.66, 14.06. IR (ATR, cm^{-1}): 2958, 2925, 2854, 1648, 1592, 1523, 1467, 1441, 1334, 1247, 1112, 862, 839, 723, 557. Yield: 67%. Anal. Calcd for $C_{44}H_{76}F_6NO_4P$: C% 63.82, H% 9.25, N% 1.69. Anal. Found: C% 63.47, H% 9.56, N% 1.63.

3c: ^{1}H-NMR ($CDCl_3$, 300 MHz): 8.52 (d, *J* = 6.7 Hz, 2H); 7.23 (m, 2H); 6.63 (s, 2H); 5.48 (s, 2H); 4.21 (t, *J* = 6.4 Hz, 2H); 3.94 (m, 6H), 1.73 (m, 8H); 1.26 (m, 56H); 0.87 (m, 12H). ^{13}C-NMR ($CDCl_3$, 75 MHz): 170.56, 154.03, 145.22, 139.24, 126.99, 113.70, 107.65, 73.44, 71.54, 69.38, 63.54, 31.91, 31.84, 30.31, 29.73, 29.64, 29.36, 29.15, 28.37, 26.08, 25.60, 22.68, 14.10. IR (ATR, cm^{-1}): 2958, 2922, 2851, 1648, 1591, 1524, 1468, 1442, 1334, 1250, 1111, 864, 833, 721, 557. Yield: 72%. Anal. Calcd for $C_{52}H_{92}F_6NO_4P$: C% 66.42, H% 9.86, N% 1.49. Anal. Found: C% 66.08, H% 10.15, N% 1.28.

3d: ^{1}H-NMR ($CDCl_3$, 300 MHz): 8.47 (d, *J* = 7.3 Hz, 2H); 7.22 (d, *J* = 7.3 Hz, 2H); 6.60 (s, 2H); 5.37 (s, 2H), 4.20 (t, *J* = 6.4 Hz, 2H); 3.93 (q, *J* = 6.6 Hz, 6H); 1.84–1.68 (m, 8H); 1.26 (m, 72H); 0.87 (t, *J* = 6.6 Hz, 12H). ^{13}C-NMR ($CDCl_3$, 75 MHz): 170.61, 154.05; 145.07, 139.23, 127.00, 113.71, 107.55, 73.45, 71.52, 69.34, 31.93, 30.34, 29.75; 29.62, 29.54, 29.38, 29.18, 28.39, 26.10, 25.62; 22.69; 14.10. IR (ATR, cm^{-1}): 2957, 2920, 2851, 1647, 1592, 1522, 1468, 1442, 1334, 1252, 1115, 846, 830, 721, 558. Yield: 67%. Analytical data reported in [28].

3e: ^{1}H-NMR ($CDCl_3$, 300 MHz): 8.51 (d, *J* = 6.8 Hz, 2H); 7.22 (d, *J* = 6.8 Hz, 2H); 6.61 (s, 2H); 5.40 (s, 2H), 4.22 (t, *J* = 6.4 Hz, 2H); 3.96–3.89 (m, 6H); 1.78 (m, 8H), 1.45–1.25 (m, 88H); 0.88 (t, *J* = 6.2 Hz, 12H). ^{13}C-NMR ($CDCl_3$, 75 MHz): 170.58, 154.03, 145.12, 139.18, 127.07, 113.69, 107.54, 73.43, 71.51, 69.33, 63.54, 31.93, 30.34, 29.74, 29.55, 29.45, 29.19, 28.39, 26.11, 25.62, 22.68, 14.10. IR (ATR, cm^{-1}): 2956, 2920, 2850, 1648, 1593, 1522, 1468, 1443, 1335, 1252, 1117, 831, 721, 558. Yield: 74%. Anal. Calcd for $C_{68}H_{124}F_6NO_4P$: C% 70.12, H% 10.73, N% 1.20. Anal. Found: C% 70.37, H% 10.99, N% 1.06.

3. Results and Discussion

3.1. Synthesis and Characterization

The synthetic procedure employed for the preparation of the pyridinium salts with side alkyl chains of the same length is depicted in Scheme 1. The starting 4-pyridone compounds **1a**–**f** were prepared by the *N*-alkylation of 4-hydroxypyridine based on the protocol reported elsewhere by us [28–31]. Subsequent *O*-alkylation with alkyl bromides in refluxing acetonitrile and in the presence of K_2CO_3 gave the bromide pyridinium salts **2a**–**e** in good yields of 67–81%. Salt metathesis of bromide salts **2a**–**e** in methanol with ammonium hexafluorophosphate produced the related pyridinium salts **3a**–**e**. The pyridinium salts **2a**–**e** and **3a**–**e** were characterized by ^{1}H-NMR and ^{13}C-RMN spectroscopy and IR spectroscopy. NMR spectroscopy is a useful tool to monitor the metathesis of the bromide ion with other various anions. For example, the ^{1}H-NMR spectra recorded in deuterated chloroform for pyridinium salts showed that the counterion nature has a pronounced impact on the chemical shift of the two protons located in the vicinity of the pyridinium nitrogen atom. While for bromide salts **2a**–**e**, the signal corresponding to these two protons in question was located around 9.17–9.24 ppm, upfield shifts in the 8.47–8.62 ppm range were observed for the ILCs with PF_6^- anion **3a**–**e**. The chemical shifts followed the order $Br^- > PF_6^-$, similar to other studies performed for different series of simple pyridinium or imidazolium when the formation of hydrogen bonds with the respective counterion can explain these observations (Figure 1) [23]. The metathesis reaction of the bromide anion with PF_6^- counterion was also confirmed by IR spectroscopy. Analysis of the IR spectra recorded for the pyridinium salts revealed that characteristic strong frequencies for the new PF_6^- group were found in the 830–840 and 550–560 cm^{-1} ranges (Figure 2).

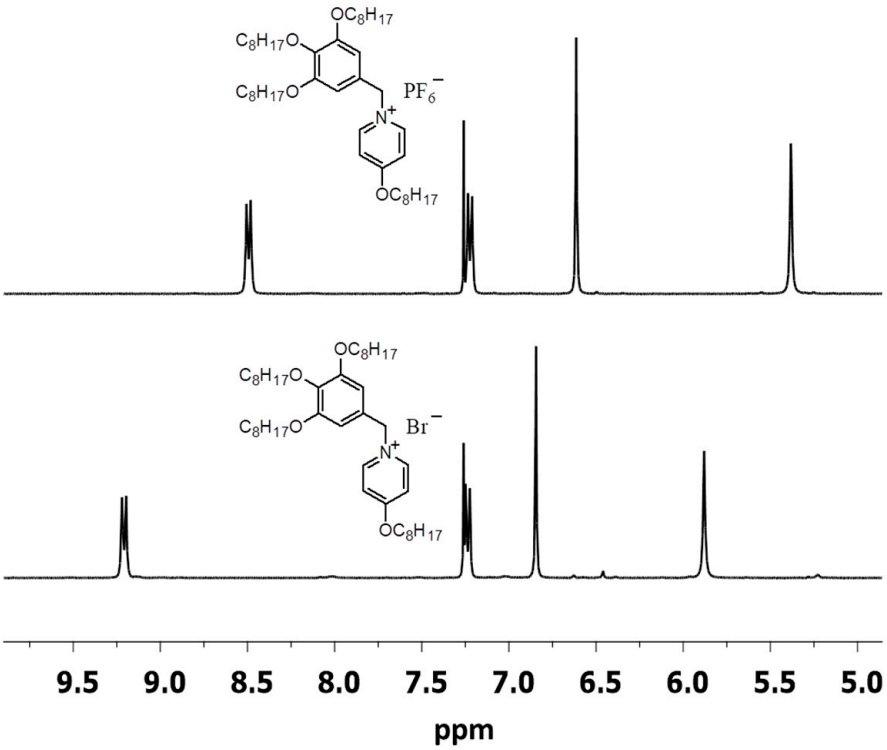

Figure 1. Low field region of the ^{1}H-NMR spectra of **2b** (Br^-) and **3b** (PF_6^-).

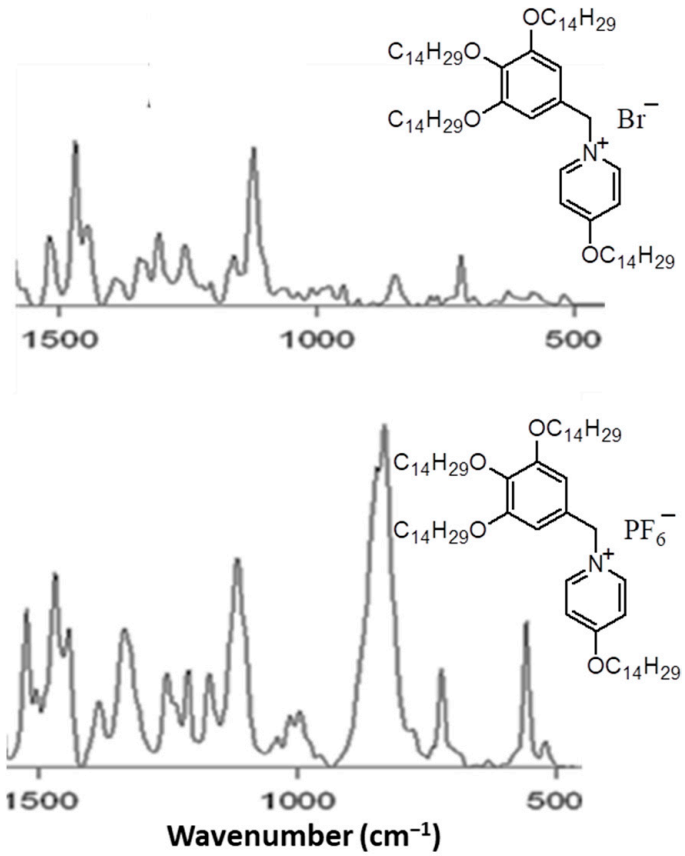

Figure 2. IR spectra (1500–500 cm^{-1} region) of **2e** (Br^-) and **3e** (PF_6^-).

3.2. Mesomorphic Properties of Pyridinium Salts

The liquid crystal properties were investigated by differential scanning calorimetry (DSC), the mesophases presented by the pyridinium salts being identified based on the characteristic textures observed by polarizing optical microscopy (POM), and the correct attribution being subsequently confirmed by powder X-ray diffraction at different temperatures (XRD). The results of the DSC measurements (transition temperatures and the related enthalpies) for all pyridinium salts are presented in Table 1. The pyridinium salts with bromide anion and alkyl chains longer than C_{10} exhibit an enantiotropic columnar phase assigned based on the characteristic texture observed by POM on cooling from the isotropic phase. In the first DSC heating run of C_6 bromide salt (**2a**), only an endothermic melting transition at 31 °C was observed. This compound melts straight to the isotropic phase and no other transitions were observed during the subsequent cooling or heating runs. The same behavior was evidenced for C_8 salt (**2b**). In the cooling run the glass transition was observed at −12 °C. The C_{10} salt (**2c**) melted to the isotropic phase at 60 °C. In addition, the second heating-cooling cycle of the C_{10} bromide analogue showed on heating a cold crystallization transition at 22 °C and the melting transition to the isotropic state at 60 °C (Figure 3a).

The second heating-cooling cycle of the pyridinium salts from the isotropic state revealed a good reproducibility of the mesophase. The mesomorphic behavior of the pyridinium salt **2d** was fully characterized by us in a previous study [28]. Similar to compound **2d**, the C_{14} pyridinium salt (**2e**) showed two separate LC phases. The transition between the two mesophases was sharp and easily observed by POM (Figure 4) and DSC (Figure 3b). The low temperature mesophase was stable down to 23 °C for **2d** and to 31 °C for **2e**. It was observed that the clearing temperature of the bromide salts depended strongly on the number of carbon atoms of the terminal aliphatic chains. The lowest isotropization temperature was recorded for the shortest analogue **2a** with six carbon atoms in the alkyl

chains and it increased with increasing the elongation of the alkyl chain. The same trend was observed for pyridinium salts with PF_6^- counterion **3a**–**e**. Moreover, the transition temperatures to the isotropic phase were found to be significantly lower in comparison to related bromide compounds **2a**–**e**.

Table 1. Transition temperatures (in °C) and enthalpies (kJ/mol) for the pyridinium salts.

Compound	Heating/Cooling Scans
2a	Cr 31 (6.7) Iso
2b	Cr 38 (3.7) Iso-12 g
2c	Cr 60 (74.3) Iso 9 (13.8) Cr
2d	Cr 62 (88.1) Col 108 (0.9) Iso 105 (0.9) Col 74 (1.4) L_{Col} 23 (18.2) Cr
2e	Cr_1 73 (136) L_{Col} 125 (0.3) Col 130 (0.4) Iso 129 (0.3) Col 118 (0.3) L_{Col} 31 (37.4) Cr_2 14 (4.5) Cr_1
3a	Cr 46 (15.9) Iso-9 g
3b	Cr 48 (21.0) Iso-4 g
3c	Cr_1 52 (0.4) Cr_2 61 (116.6) Iso 2 (7.1) Cr_1
3d	Cr 72 (80.5) Iso 26 (35.2) Cr
3e	Cr_1 81 (63.4) Cr_2 87 (36.3) Iso 56 (63.1) Cr_2

The corresponding enthalpies are given in parenthesis: Cr_1; Cr_2—crystalline phases; g—glassy state; Iso—isotropic phase; Col—columnar phase; L_{Col}—lamello-columnar phase.

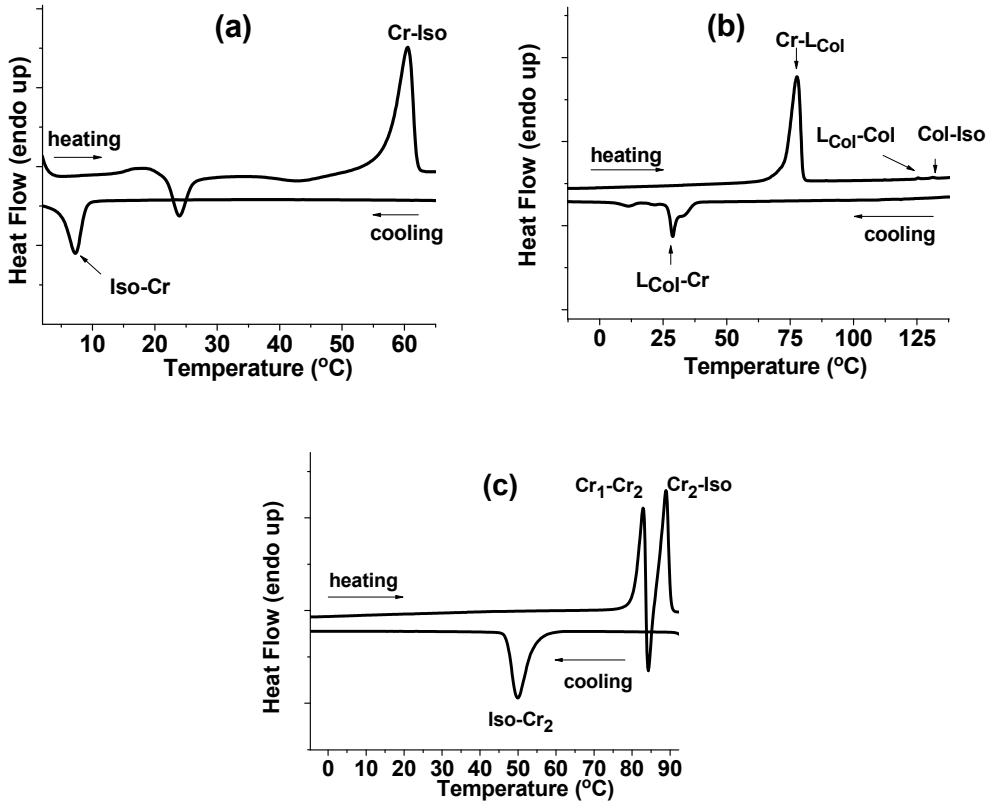

Figure 3. Second heating-cooling DSC thermogram for **2b** (**a**), **2e** (**b**) and **3e** (**c**).

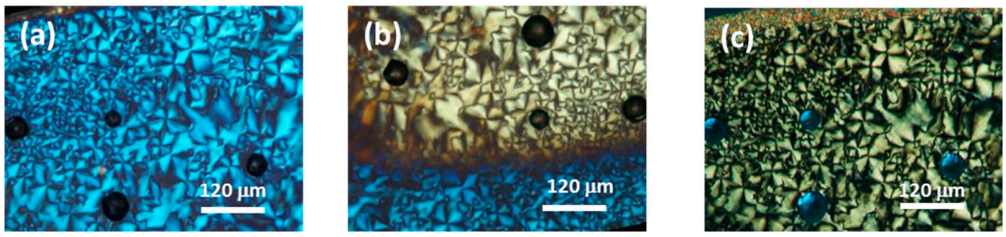

Figure 4. POM pictures for compound **2e** at cooling from the isotropic liquid at 125 °C (**a**), 117 °C (the transition between the two columnar mesophases) (**b**), 55 °C (**c**).

Deceptively, the pyridinium salts with the PF_6^- counterion, **3a–e,** did not exhibit liquid crystal properties. For these compounds, the formation of liquid crystal phases was strongly influenced by the separation between the pyridinium ionic fragments and the hydrophobic aliphatic chains and, obviously, the counterion had a major influence on the stabilization of the mesophase. For example, a similar significant effect of the counterions was found in the related methylimidazolium salts with the 3,4,5-tris(alkyloxy)benzyl mesogenic groups [32].

The tentative assignment of the mesophases was confirmed from data analysis obtained by X-ray powder diffraction, recorded at different temperatures (Figure 5 and Table 2). The diffractograms of **2d** and **2e** recorded at 80 °C and 120 °C, respectively, showed only one peak in the small-angle region, with no other significant features. By correlating the XRD information with the optical observations at the polarizing optical microscope, a hexagonal columnar phase could be assigned to the LC phases observed at higher temperatures on cooling from the isotropic state. For the calculation of the number of molecules per column unit, the following relations were used: $N = V_{cell}/V_{mol}$, where $V_{cell} = S_{col}xh$ (assuming that h~4.5 Å, $S_{col} = \sqrt{3}a^2/2$ and $V_{mol} = M_w/(N_A \cdot \rho)$; and M_w is the molecular weight, ρ is the density and it was approximated to 1 $g \cdot cm^{-3}$ and N_A is the Avogadro' number). Given an interplanar distance of 25.44 Å (d_{100}) for **2d**, and 27.51 Å for **2e** and the corresponding lattice parameter (a = 29.38 and 31.77 Å for **2d** and **2e**, respectively), then the discs are composed of two molecules of pyridinium salts having (N~2.23 and 2.15 for **2d** and **2e**, respectively), in total, eight alkyl chains at the periphery. The columnar organization can be regarded as the accumulation of two pyridinium cationic units which produces a disk-like arrangement with a parallel charge alternation to the normal of the 2D hexagonal lattice. In addition, the pyridinium salts with the highest number of carbon atoms (C_{12}—**2d** and C_{14}—**2e**) exhibited an additional mesophase at a lower temperature. While the POM observations showed a change of color but no significant textural modifications, the XRD patterns recorded at the lower temperature display a major transformation. The corresponding diffractogram of **2e** recorded at 60 °C clearly display a series of five lines that can be indexed as d_{001}, d_{002}, d_{003}, d_{004} and d_{007} of a lamellar organization. The sharpness of the small-angle peaks indicates the long range of the lamellar ordering and the 2D arrangement of the columns. No additional peak at higher angles that are correlated with the intracolumnar distances (~3.5 Å) could be observed, and, thus, a columnar lamellar organization with a certain degree of the disorder may be assumed for this LC phase [33–36]. In addition, the shift to a higher angle concomitant with the sharpening of the high-angle diffraction peak might indicate the closer molecular lateral packing of the molecules associated with columnar stacking within the layers [37,38].

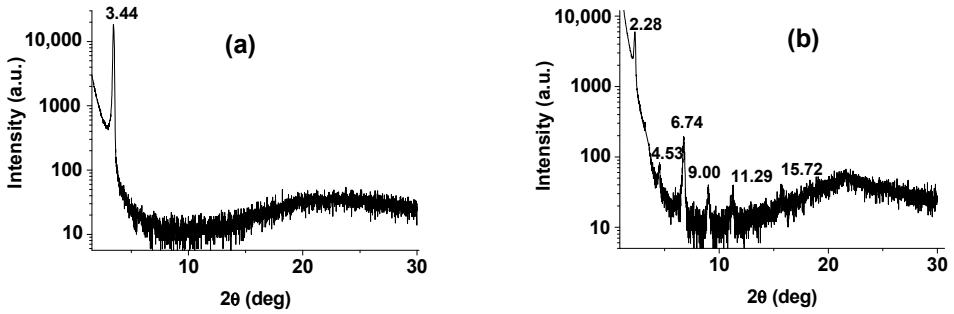

Figure 5. XRD patterns of **2e** at 120 °C (**a**) and at 50 °C (**b**).

Table 2. XRD data for bromide salts **2d** and **2e**.

Compound	Mesophase	T/°C	Indexation	D-Spacing obs./Å	D-Spacing calc./Å	Lattice Parameters/Å [b]
2d	Col	80	100 Broad [c]	25.44 4.5	25.44	a = 29.38
2e	Col	120 [a]	100	27.51	27.51	a = 31.77
/	/	/	Broad [c]	4.5	/	/
/	L_{Col}	60	001	39.76	39.76	/
/	/	/	002	19.75	19.88	/
/	/	/	003	13.12	13.25	/
/	/	/	004	9.84	9.94	/
/	/	/	007	5.62	5.68	/
/	/	/	Broad [c]	4.3	/	/

[a] On cooling from isotropic state. [b] The hexagonal columnar lattice parameter a = $2<d_{100}>/\sqrt{3}$. [c] Broad peak assigned to molten alkyl chains.

4. Conclusions

Anion size and chain length variation for pyridinium salts **2a**–**e** and **3a**–**e** had a serious impact on mesophase stability and temperature range. On the contrary, these factors had little effect on the mesophase type. The pyridinium salts with the larger size PF_6^- counterion, **3a**–**e,** did not exhibit liquid crystal properties. The bromide salts required a minimum length of carbon chains to display their liquid crystalline properties. Thus, salts with shorter chains C_6, C_8 and C_{10} did not show mesophase, while longer chains analogues with C_{12} and C_{14} exhibited two enantiotropic columnar phases. The lower-temperature columnar phase was found to possess long-range lamellar organization based on the presence of a series of equidistant peaks in the low angle region of the XRD pattern. The C_{12} family of pyridinium salts with various counterions (Br^-, NO_3^-, BF_4^- and PF_6^-) reported earlier showed that only the bromide salt displayed mesomorphic behavior. Thus, the present work provides experimental evidence to confirm that the elongation of alkyl chains in these pyridinium salts is not enough to compensate for the destabilization of the mesophase by the inclusion of larger sized counterions.

Author Contributions: Conceptualization, V.C.; methodology, V.C., D.M.-M. and M.I.; validation, V.C., I.P., M.M. and T.S.; formal analysis, I.D., I.P. and F.L.C.; investigation, F.L.C., M.M., I.D. and M.I.; writing—original draft preparation, F.L.C. and V.C.; writing—review and editing, V.C.; supervision, V.C. All authors have read and agreed to the published version of the manuscript.

Funding: DMM acknowledges the support of the PubArt project.

Data Availability Statement: Not applicable.

Conflicts of Interest: The authors declare no conflict of interest.

References

1. Goossens, K.; Lava, K.; Bielawski, C.W.; Binnemans, K. Ionic liquid crystals: Versatile materials. *Chem. Rev.* **2016**, *116*, 4643–4807. [CrossRef] [PubMed]
2. Chen, S.; Eichhorn, S.H. Ionic discotic liquid crystals. *Israel J. Chem.* **2012**, *52*, 830–843. [CrossRef]
3. Dong, K.; Zhang, S. Hydrogen bonds: A structural insight into ionic liquids. *Chem. Eur. J.* **2012**, *18*, 2748–2761. [CrossRef] [PubMed]
4. Hunt, P.A.; Ashworth, C.R.; Matthews, R.P. Hydrogen bonding in ionic liquids. *Chem. Soc. Rev.* **2015**, *44*, 1257–1288. [CrossRef]
5. Ma, Y.; Liu, Y.; Su, H.; Wang, L.; Zhang, J. Relationship between hydrogen bond and viscosity for a series of pyridinium ionic liquids: Molecular dynamics and quantum chemistry. *J. Mol. Liq.* **2018**, *255*, 176–184. [CrossRef]
6. Faul, C.F.J.; Antonietti, M. Ionic self-assembly: Facile synthesis of supramolecular materials. *Adv. Mater.* **2003**, *15*, 673–683. [CrossRef]
7. Axenov, K.V.; Laschat, S. Thermotropic ionic liquid crystals. *Materials* **2011**, *4*, 206–259. [CrossRef]
8. Fernandez, A.A.; Kouwer, P.H. Key developments in ionic liquid crystals. *Int. J. Mol. Sci.* **2016**, *17*, 731. [CrossRef]
9. Binnemans, K. Ionic liquid crystals. *Chem. Rev.* **2005**, *105*, 4148–4204. [CrossRef]
10. Nelyubina, Y.V.; Shaplov, A.S.; Lozinskaya, E.I.; Buzin, M.I.; Vygodskii, Y.S. A new volume-based approach for predicting thermophysical behavior of ionic liquids and ionic liquid crystals. *J. Am. Chem. Soc.* **2016**, *138*, 10076–10079. [CrossRef]
11. Neidhardt, M.M.; Wolfrum, M.; Beardsworth, S.; Wöhrle, T.; Frey, W.; Baro, A.; Stubenrauch, C.; Giesselmann, F.; Laschat, S. Tyrosine-based ionic liquid crystals: Switching from a smectic a to a columnar mesophase by exchange of the spherical counterion. *Chem. Eur. J.* **2016**, *22*, 16494–16504. [CrossRef] [PubMed]
12. Cao, W.; Senthilkumar, B.; Causin, V.; Swamy, V.P.; Wang, Y.; Saielli, G. Influence of the ion size on the stability of the smectic phase of ionic liquid crystals. *Soft Matter* **2020**, *16*, 411–420. [CrossRef] [PubMed]
13. Liu, S.; Yan, G.; Wang, J.; Zhou, J.; Bie, L.; Jia, Y.; Meng, F. Self-assembly, phase behaviour and ion-conducting property of pyridinium-based ionic liquid-crystalline oligomers. *Liq. Cryst.* **2021**, *48*, 201–214. [CrossRef]
14. Wang, R.-T.; Tsai, S.-J.J.; Lee, G.-H.; Lai, C.K. Aggregation-induced emissions in columnar wedge-shaped pyridinium-based ionic liquid crystals. *Dyes Pigments* **2020**, *173*, 107913. [CrossRef]
15. Tang, X.; Bai, L.; Kong, S.; Wang, X.; Meng, F. Multi-arm ionic liquid crystals formed by cholesteric mesophase and pyridinium groups. *Liq. Cryst.* **2019**, *46*, 1252–1265. [CrossRef]
16. Jo, T.S.; Han, H.; Bhowmik, P.K.; Heinrich, B.; Donnio, B. Thermotropic liquid-crystalline and light-emitting properties of poly(pyridinium) salts containing various diamine connectors and hydrophilic macrocounterions. *Polymers* **2019**, *11*, 851. [CrossRef]
17. Wang, X.; Bai, L.; Kong, S.; Song, Y.; Meng, F. Star-shaped supramolecular ionic liquid crystals based on pyridinium salts. *Liq. Cryst.* **2019**, *46*, 512–522. [CrossRef]
18. Ali, M.O.; Pociecha, D.; Wojciechowski, J.; Novozhilova, I.; Friedli, A.C.; Kaszyński, P. Highly quadrupolar derivatives of the [closo-B10H10]2-anion: Investigation of liquid crystalline polymorphism in an homologous series of 1,10-bis(4-alkoxypyridinium) zwitterions. *J. Organomet. Chem.* **2018**, *865*, 226–233. [CrossRef]
19. Wang, R.-T.; Lee, G.-H.; Lai, C.K. Effect of counter ions on the mesogenic ionic: N–phenylpyridiniums. *CrystEngComm* **2018**, *20*, 2593–2607. [CrossRef]
20. Luo, J.; Zhang, L.; Lu, J.; Bai, L.; He, X.; Meng, F. Polymerised ionic liquid crystals bearing imidazolium and bipyridinium groups. *Liq. Cryst.* **2017**, *44*, 1293–1305. [CrossRef]
21. Zhao, D.; Zhang, L.; Bai, L.; Luo, J.; He, X.; Meng, F.-B. Synthesis and characterization of liquid-crystalline ionomers with pendant cholesteryl pyridinium salt mesogens. *RSC Adv.* **2016**, *6*, 26791–26799. [CrossRef]
22. Bhowmik, P.K.; Al-Karawi, M.K.M.; Killarney, S.T.; Dizon, E.J.; Chang, A.; Kim, J.; Chen, S.L.; Principe, R.C.G.; Ho, A.; Han, H.; et al. Thermotropic liquid-crystalline and light-emitting properties of Bis(4-aalkoxyphenyl) viologen Bis(triflimide) salts. *Molecules* **2020**, *25*, 2435. [CrossRef] [PubMed]
23. Kohnen, G.; Tosoni, M.; Tussetschläger, S.; Baro, A.; Laschat, S. Counterion effects on the mesomorphic properties of chiral imidazolium and pyridinium ionic liquids. *Eur. J. Org. Chem.* **2009**, *32*, 5601–5609. [CrossRef]
24. Tosoni, M.; Laschat, S.; Baro, A. Synthesis of novel chiral ionic liquids and their phase behavior in mixtures with smectic and nematic liquid crystals. *Helv. Chim. Acta* **2004**, *87*, 2742–2749. [CrossRef]
25. Kapernaum, N.; Lange, A.; Ebert, M.; Grunwald, M.A.; Haege, C.; Marino, S.; Zens, A.; Taubert, A.; Giesselmann, F.; Laschat, S. Current topics in ionic liquid crystals. *ChemPlusChem* **2022**, *87*, e2021003. [CrossRef] [PubMed]
26. Cîrcu, V. *Progress and Developments in Ionic Liquids*; Handy, S., Ed.; IntechOpen: London, UK, 2017; pp. 285–311.
27. Lu, J.T.; Lee, C.K.; Lin, I.J. Ionic liquid crystals derived from 4-hydroxypyridine. *Soft Matter* **2011**, *7*, 3491–3501. [CrossRef]
28. Pana, A.; Badea, F.L.; Ilis, M.; Staicu, T.; Micutz, M.; Pasuk, I.; Cîrcu, V. Effect of counterion on the mesomorphic behavior and optical properties of columnar pyridinium ionic liquid crystals derived from 4-hydroxypyridine. *J. Mol. Struct.* **2015**, *1083*, 245–251. [CrossRef]
29. Chiriac, L.F.; Pasuk, I.; Secu, M.; Micutz, M.; Cîrcu, V. Wide-range columnar and lamellar photoluminescent liquid-crystalline lanthanide complexes with mesogenic 4-pyridone derivatives. *Chem. Eur. J.* **2018**, *24*, 13512–13522. [CrossRef]

30. Chiriac, F.L.; Iliş, M.; Madalan, A.; Manaila-Maximean, D.; Secu, M.; Cîrcu, V. Thermal and emission properties of a series of lanthanides complexes with N-biphenyl-alkylated-4-pyridone ligands: Crystal structure of a terbium complex with N-benzyl-4-pyridone. *Molecules* **2021**, *26*, 2017. [CrossRef]
31. Pană, A.; Chiriac, F.L.; Secu, M.; Pasuk, I.; Ferbinteanu, M.; Micutz, M.; Cîrcu, V. A new class of thermotropic lanthanidomesogens: Eu(III) nitrate complexes with mesogenic 4-pyridone ligands. *Dalton Trans.* **2015**, *44*, 14196–14199. [CrossRef]
32. Yoshio, M.; Ichikawa, T.; Shimura, H.; Kagata, T.; Hamasaki, A.; Mukai, T.; Ohno, H.; Kato, T. Columnar liquid-crystalline imidazolium salts. Effects of anions and cations on mesomorphic properties and ionic conductivities. *Bull. Chem. Soc. Jpn.* **2007**, *80*, 1836–1841. [CrossRef]
33. Cuerva, C.; Campo, J.A.; Cano, M.; Schmidt, R. Lamellar columnar liquid-crystalline mesophases as a 2D platform for anhydrous proton conduction. *J. Mater. Chem. C* **2019**, *7*, 10318–10330. [CrossRef]
34. Veltri, L.; Maltese, V.; Auriemma, F.; Santillo, C.; Cospito, S.; la Deda, M.; Chidichimo, G.; Gabriele, B.; de Rosa, C.; Beneduci, A. Mesophase tuning in discotic dimers π-conjugated ionic liquid crystals through supramolecular interactions and the thermal history. *Cryst. Growth Des.* **2016**, *16*, 5646–5656. [CrossRef]
35. Abe, Y.; Takagi, Y.; Nakamura, M.; Takeuchi, T.; Tanase, T.; Yokokawa, M.; Mukai, H.; Megumi, T.; Hachisuga, A.; Ohta, K. Structural, photophysical, and mesomorphic properties of luminescent platinum(II)-salen Schiff base complexes. *Inorg. Chim. Acta* **2012**, *392*, 254–260. [CrossRef]
36. Malthete, J.; Nguyen, H.T.; Destrade, C. Phasmids and polycatenar mesogens. *Liq. Cryst.* **1993**, *13*, 171–187. [CrossRef]
37. Choi, Y.-J.; Kim, D.-Y.; Park, M.; Yoon, W.-J.; Lee, Y.; Hwang, J.-K.; Chiang, Y.-W.; Kuo, S.-W.; Hsu, C.-H.; Jeong, K.-U. Self-assembled hierarchical superstructures from the benzene-1,3,5-tricarboxamide supramolecules for the fabrication of remote-controllable actuating and rewritable films. *ACS Appl. Mater. Interfaces* **2016**, *8*, 9490–9498. [CrossRef]
38. Beneduci, A.; Cospito, S.; Crispini, A.; Gabriele, B.; Nicoletta, F.P.; Veltri, L.; Chidichimo, G. Switching from columnar to calamitic mesophases in a new class of rod-like thienoviologens. *J. Mater. Chem. C* **2013**, *1*, 2233–2240. [CrossRef]